Cancer Chemother Pharmacol (2012) 69:1567–1582
DOI 10.1007/s00280-012-1863-5

ORIGINAL ARTICLE

Novel physiologically based pharmacokinetic modeling of patupilone for human pharmacokinetic predictions

Binfeng Xia · Tycho Heimbach · Tsu-han Lin · Handan He · Yanfeng Wang · Eugene Tan

Received: 12 October 2011 / Accepted: 18 March 2012 / Published online: 11 April 2012

Abstract
Purpose Patupilone (EPO906) is a novel potent microtubule stabilizer, which has been evaluated for cancer treatment. A novel physiologically based pharmacokinetics (PBPK) model was developed based on nonclinical data to predict the disposition of patupilone in cancer patients.
Methods After a single intravenous dose (1.2 mg/kg) in male Han–Wistar rats, the tissue distribution of ^{14}C-patupilone was investigated by quantitative whole-body autoradiography (QWBA). The blood radioactivity and patupilone concentration were determined by LC–MS/MS and liquid scintillation counting. A novel PBPK model was developed based on rat tissue concentration data to predict blood concentration–time profiles of patupilone in cancer patients. PBPK parameters derived from the rat were applied to a human PBPK model. Phase I clinical pharmacokinetic data in Caucasian and Japanese cancer patients at various doses ranging from 0.75 to 10 mg/m^2 were successfully described using the PBPK approach.
Results Patupilone dispositions in lung, heart, muscle, spleen, liver, brain, adipose, and testes of rats were well described using the PBPK model developed assuming a perfusion rate-limited distribution between different compartments. For skin and bone marrow, concentration–time profiles were modeled assuming a permeability-limited distribution between different compartments. The simulated human pharmacokinetic profiles from the PBPK model showed good agreement with observed clinical pharmacokinetic data, where the model predicted AUC, $t_{1/2}$, V_{ss}, and CL values were within approximately twofold of the observed values for all dose groups.
Conclusions The distribution of patupilone in rats was well described by a PBPK model based on measured tissue distribution profiles generated by QWBA combined with metabolism data. The human PBPK model adequately predicted blood pharmacokinetics of patupilone in cancer patients. The PBPK model based upon preclinical tissue distribution data can aid in successful prediction of pharmacokinetics in humans.

Keywords Patupilone · Physiologically based pharmacokinetics · Human PBPK modeling · Quantitative whole-body autoradiography · Tissue distribution · GastroPlus

Introduction

Epothilones are a new class of natural microtubule-targeting cytotoxic agents isolated from the myxobacterium *Sorangium cellulosum*, which have shown cytotoxic activity in human cancer cell lines [1]. An analog of epothilones, patupilone (epothilone B: EPO906), is currently an investigational agent in clinical development for the treatment of second-line ovarian cancer. Patupilone induces mitotic cell cycle arrest and eventual apoptosis in human cancer cells by microtubule stabilization and suppression of microtubule dynamics. Patupilone binds to the same molecular target of β-tubulin as taxanes but has a higher binding affinity than paclitaxel or docetaxel [1, 6, 30]. Patupilone, unlike paclitaxel, is not a substrate of the efflux transporter

B. Xia · T. Heimbach (✉) · T. Lin · H. He
Department of Drug Metabolism and Pharmacokinetics, Novartis Institutes for Biomedical Research, East Hanover, NJ 07936, USA
e-mail: tycho.heimbach@novartis.com

Y. Wang · E. Tan
Department of Clinical Pharmacology, Oncology, Novartis Pharmaceuticals Corporation, Florham Park, NJ 07932, USA

P-glycoprotein (P-gp) and thereby retains its inhibitory activity against paclitaxel-resistant cancer cells over-expressing P-gp [4]. In rodents, patupilone showed sustained anticancer effect in multidrug-resistant tumors, whereas paclitaxel has no significant effect [22]. Its antitumor activity has been demonstrated in several clinical trials with a number of tumor types, including ovarian, prostate, lung, and colon cancers [3, 7, 8, 12, 19, 37, 39].

Patupilone pharmacokinetics have been previously studied in mice [22], rats [22], dogs, and humans [22, 37, 38]. In all rodent studies, patupilone rapidly distributed to all tissues and was eliminated from blood, with long retention in organs including muscle, liver, and brain [22, 37]. Similarly, the human pharmacokinetics exhibited a rapid distribution and an extensive elimination phase with a half-life ($t_{1/2}$) over 100 h in clinical dose-escalation studies [37]. The pharmacokinetic behavior in human was considered to be linear as no dose dependency was found for clearance (CL), volume of distribution at steady state (V_{ss}), and $t_{1/2}$ [37]. Patupilone metabolism is characterized by hydrolytic and oxidative steps, and the lactone hydrolysis mediated by carboxyl esterase appears to be the major metabolic pathway in humans and preclinical species while oxidative metabolism of patupilone is mainly catalyzed by CYP3A4 and CYP2C19 [5, 38]. Prior pharmacokinetic studies have largely employed noncompartment models to characterize data obtained from clinical and preclinical studies. Few publications have investigated patupilone's distribution in tissues [22]; however, due to the promising cytotoxic effect of patupilone for many tumor types, patupilone dispositions in human tissues have has been of interest. To our best knowledge, there has been no prior attempt to develop a physiologically based pharmacokinetic (PBPK) model to characterize tissue disposition for epothilones. The primary objectives of our study were to: (1) determine the disposition and tissue distribution of patupilone in rats following an intravenous administration; (2) describe a rat PBPK model for patupilone to characterize the time-course of plasma and tissue exposure of patupilone; and (3) extrapolate the rat PBPK model toward the prediction of human pharmacokinetics at multiple dosing levels in Japanese and Caucasian patients. The human PBPK model may serve as the basis for assessing the pharmacokinetic and pharmacodynamic relationships in various tissues and predicting the outcome of various dosing regimen.

Methods

Preclinical and clinical pharmacokinetic data

In vitro metabolic profiles of patupilone

The main metabolism pathway of patupilone is via lactone ring hydrolysis mediated by carboxyl esterase in rat and human (Fig. 1) both in vitro and in vivo. The major metabolite of patupilone, patupilone acid, is a hydrolytic product that results from the cleavage of the lactone ester bond. Patupilone acid further undergoes epoxide hydrolysis to form a diol metabolite (Fig. 1). The physicochemical properties of these two metabolites differ from those of patupilone. At the physiological pH of 7.4, patupilone is mainly neutral (unionized), whereas the major metabolite of patupilone acid is mainly ionized. The predicted log $D_{pH=7.4}$ values for patupilone, patupilone acid, and 1,16-diol-patupilone acid were 3.1, 0.17, and −0.77 (ADMET predictor v5 Simulation Plus Inc., Lancaster, CA), respectively, suggesting that patupilone has a higher lipophilicity and distributes more broadly into tissues than its more polar metabolites.

The in vitro biostability of patupilone was investigated in liver microsome and/or plasma from rats and humans. Patupilone appeared to be stable in human plasma but not stable in rat plasma within 2 h. The metabolic kinetics of ^{14}C-patupilone was characterized in pooled human liver microsomes. The enzymatic reaction linearity for the depletion of ^{14}C-patupilone was ensured over the incubation time (40–90 min) and protein content (1.0–2.0 mg/mL). The enzyme kinetic parameters of K_m and V_{max} were determined in pooled human liver microsome (1 mg/mL) after 60 min of incubation at 37 °C with substrate concentrations ranging from 0.25 to 300 μM. Due to limited solubility of patupilone, the maximum achievable substrate

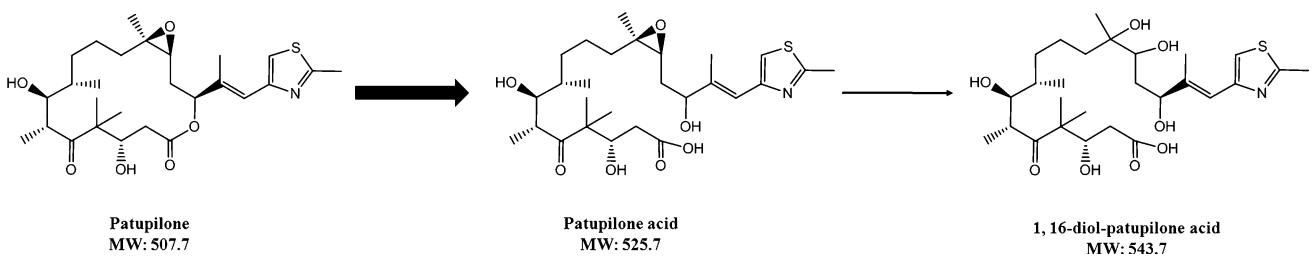

Fig. 1 Major metabolic pathway for patupilone

concentration in the incubation could not exceed 300 μM. The reaction was stopped by adding ice-cold acetonitrile, and the incubation samples were centrifuged for 15 min at 30,000*g*. The supernatant was evaporated and redissolved in 150 μL of 5 % acetonitrile. The reconstituted samples were injected into a HPLC system (Jasco, Tokyo, Japan) for the analysis of remaining substrate concentration of ^{14}C-patupilone. The HPLC method used a LiChrospher 100 RP-18 column (250 × 4 mm) and a stepwise gradient with solvent A (30 mM ammonium acetate in water) and solvent B (acetonitrile) with a flow rate of 1 mL/min. Solvent A in the gradient started at 95 % and then changed as follows: 20 % (18 min), 5 % (from 20 to 22 min), and 95 (23 min). Radioactivity in the HPLC eluent was measured on an on-line radioactivity detector (model LB508, Berthhold, Germany) to determine the concentration of ^{14}C-patupilone after the incubation. The rate of depletion of the substrate was calculated based on the following equation: Rate of depletion of substrate = (Initial concentration of patupilone − concentration of patupilone after incubation)/incubation time (60 min)/microsome protein concentration (1 mg/mL). The enzyme kinetics for the rate of depletion of ^{14}C-patupilone were analyzed by nonlinear regression analysis with a weighting factor of $1/x^2$ (x is the substrate concentration) to determine the apparent Michaelis–Menten parameters (K_m and V_{max}) of substrate depletion. The intrinsic clearance was then calculated by dividing V_{max} by K_m.

Disposition and tissue distribution of ^{14}C-patupilone in rats

All animal experimental procedures were approved by Novartis Animal Care and Use Committee. Three groups of Han–Wistar rats were used in the experiments to investigate the pharmacokinetic disposition (group A), elimination pathway (group B), and whole-body tissue distribution (group C), respectively. The methods and results for the experiments are briefly described below.

For the investigation of patupilone pharmacokinetics (group A), a single intravenous dose of 1.2 mg/kg of ^{14}C-patupilone was administrated to three Han–Wistar rats that weighed from 270 to 290 g. Blood samples (200–300 μL) were collected in micro-centrifuge tubes with an eserine-heparinized mix at 0.083, 0.25, 0.5, 1, 3, 8, 24, 48, 72, 120, and 168 h and stored at −20 °C until analysis. The total radioactivity concentrations in rat blood samples were measured by liquid scintillation counting (LSC), and the concentrations of patupilone in rat blood were determined by a reported LC–MS/MS method [22] that fulfilled with the following acceptance criteria (in-house analytical method validation protocol), including QC precision (RSD ≤ 15 %), QC accuracy (100 % − |% error| ≥ 85.0 %), stability (precision and bias ≤ ±15 % for three cycles of freeze/thaw stability at −80 °C, 12 weeks long-term stability at −20 °C, 24 h short-term stability at room temperature), and calibration curve linearity (0.1–200 ng/mL, correlation coefficient $R^2 > 0.98$). The method was acceptable according to industry guidance for bioanalytical method validation established by the FDA. The pharmacokinetic parameters for the total radiolabeled components and patupilone were calculated by noncompartmental analysis using WinNonlin Phoenix v6.1 (Pharsight, Sunnyvale, CA).

For characterization of the patupilone elimination pathway (group B), a single intravenous dose of 1.2 mg/kg of ^{14}C-patupilone was administered to three bile duct-cannulated Han–Wistar rats that weighed from 260 to 290 g. Urine, bile, and feces were collected on ice daily up to 72 h after the dosing and were stored at −80 °C until analysis. After preparation of samples, the metabolic profiles in urine, bile, and feces were determined using LC–MS/MS and HPLC-radiometry, and the recoveries of total radioactivity were measure by LSC.

In tissue distribution studies (group C), a single intravenous dose of 1.2 mg/kg of ^{14}C-patupilone was administered to the animals that weighed from 240 to 285 g. Animals were sacrificed at 0.083, 0.5, 2, 8, 24, and 72 h after the dose (one animal per time point) and were immediately deep frozen using a mixture of dry-ice and hexane at about −75 °C and then embedded in frozen blocks containing 4–5 % aqueous gelatin at −20 °C. The tissue radioactivity concentrations were then determined by quantitative whole-body auto-radioluminography (QWBA) in a number of organs and tissues, including lung, spleen, liver, adipose, muscle, heart, brain, skin, bone marrow, kidney, and reproductive organ (testis).

Phase I dose-escalation clinical trials in Caucasians and Japanese patients

Human pharmacokinetic data were obtained in two Phase I dose-escalation clinical trials in Caucasians (study 01) and Japanese (study 02) patients, respectively. Patupilone was infused intravenously (5, 15, 20, or 30 min) at various doses that ranged from 0.75 to 10 mg/m^2 (equivalent to 0.02–0.27 mg/kg, assuming a 1 mg/kg is equivalent to a 37 mg/m^2). In brief, eligibility criteria for study 01 and 02 included a histologically documented advanced solid tumor, who had failed at least one standard systemic therapy or for whom standard systemic therapy did not exist: male or female patients ≥18 (study 01) or 20 (study 02) years of age; World Health Organization (WHO) performance status score of ≤1 (study 02) or 2 (study 01) with a life expectancy ≥3 months; absolute neutrophil count ≥1.5 × 10^9/L (study 01) or 2 × 10^9/L (study 02); hemoglobin ≥9.5 g/dL (study 02); platelet count ≥100 × 10^9/L; total bilirubin ≤1.5 the upper limit of normal (ULN);

aspartate and alanine transaminase ≤2.5 ULN. Patients were excluded if they were pregnant or breast-feeding, had severe and/or uncontrolled medical conditions, had received any investigational drug, chemotherapy, radiation therapy within 28 days prior to study entry, or had other noncompliant conditions for the studies. The study was approved by the respective institutional review boards and conducted in accordance with the principle of Declaration of Helsinki and the International Conference on Harmonization guidelines on Good Clinical Practice.

In both studies, blood and urine samples were collected up to 21 days (504 h) and 48 h post-dose, respectively. The blood and urine concentrations of patupilone were measured by LC–MS/MS as published previously [35]. The method fulfilled with the same acceptance criteria as the method for the determination of patupilone concentration in rat blood. The method met all criteria according to industry guidance for bioanalytical method validation established by the FDA. The pharmacokinetic parameters of patupilone were calculated by noncompartmental analysis using WinNonlin Phoenix v6.1.

Modeling and simulations

PBPK models development in rats

The QWBA radioactivity concentration (Fig. 2a) can be assumed to reflect the tissue concentrations of patupilone for the following two reasons: (1) patupilone exhibited a low blood clearance (0.33 L/h/kg) corresponding to ~10 % of the rat hepatic blood flow (3.3 L/h/kg) and was also the major circulation components in blood with much higher systemic exposure than its metabolites (see "Results"); (2) patupilone is a neutral compound, whereas the major metabolite of patupilone acid is ionized at physiological pH, and patupilone is more lipophilic than the major metabolite of patupilone acid as well as its subsequent metabolites based on predicted log $D_{pH=7.4}$ value. Therefore, it is safe to assume that patupilone distributes more broadly into tissues, whereas the polar metabolites are very hydrophilic and have very limited permeation across cell membranes. The concentrations of patupilone in several selected organs (e.g., liver, brain, and muscle) after tissue dissection had been previously

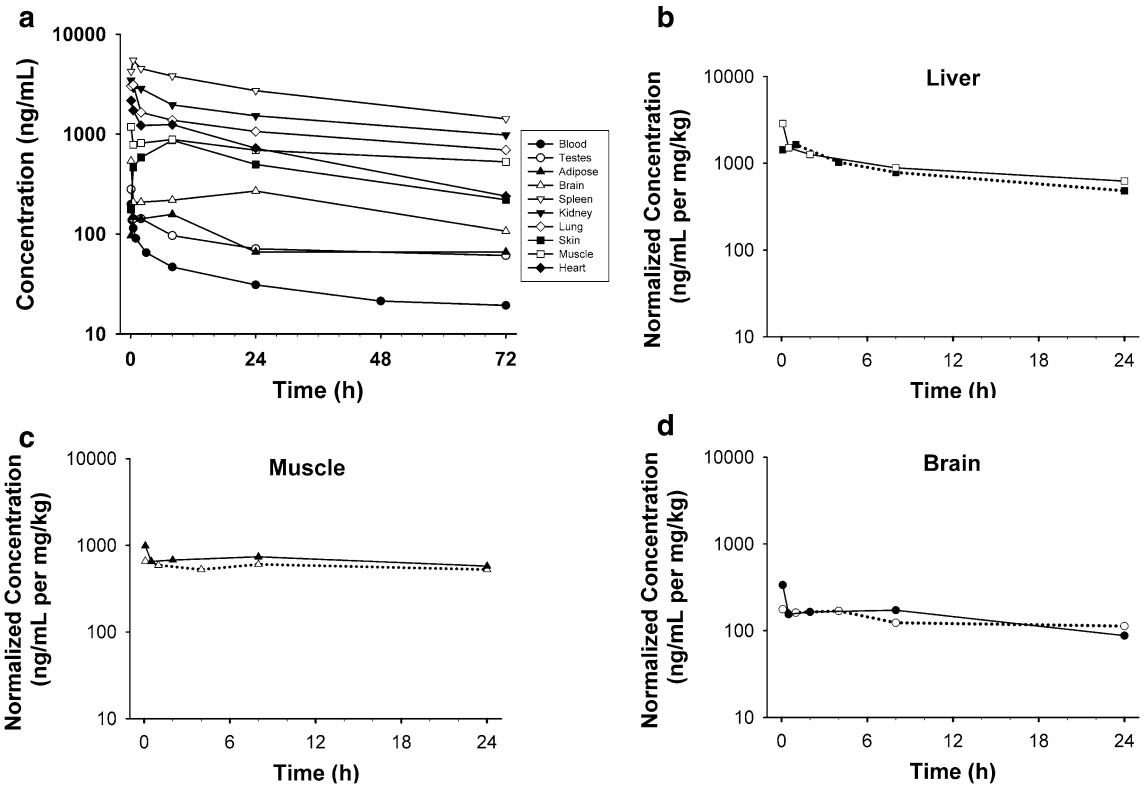

Fig. 2 **a** Tissue radioactivity concentrations of patupilone from the rat QWBA study after a single i.v. administration of 1.2 mg/kg of ^{14}C-patupilone. **b–d** Observed tissue concentrations of patupilone (*opened symbols*) after a single intravenous dose of 1.5 mg/kg in rats [22] and QWBA radioactivity concentrations (*solid symbols*) from the rat QWBA data (1.2 mg/kg, i.v.). The dose-normalized concentrations were presented in **b–d**

determined by LC–MS/MS method at a dose of 1.5 mg/kg as reported by O'Reilly et al. [22]. The tissue concentrations measured by LC–MS/MS method were very similar to the QWBA radioactivity concentrations after dose normalization (Fig. 2b–d). Therefore, the QWBA radioactivity tissue concentrations were used to fit the rat PBPK model.

Hydrolysis of the lactone to the carboxylate forms of patupilone in blood was not considered in the modeling efforts. It appeared that this transition was not significant as patupilone blood concentrations represented most of the blood radiolabeled components at all time points (see "Results"). In addition, the concentrations in most of the tissues (e.g., liver, muscle, brain, etc.) were higher than the plasma concentration and declined very slowly with a long termination half-life (Fig. 2a). Further, urinary excretion was found a minor elimination pathway for radioactivity (<5 % recovery of total radioactivity dose) while metabolites of patupilone were mainly detected in bile (see "Results"), suggesting liver was still the major elimination organ for patupilone. Overall, it was assumed that extrahepatic metabolism was insignificant, and elimination of patupilone was via the liver.

A schematic diagram of the PBPK model for patupilone in male Han–Wistar rats is presented in Fig. 3a, which consists of 12 compartments including gut, lung, liver, spleen, adipose, muscle, heart, brain, kidney, skin, reproductive organs (testes), and bone marrow. The tissue/organ compartments were linked to the venous and arterial blood circulation, and physiological parameters are listed in Table 1. The sum of the tissue volumes accounted for ~85 % of the average rat body weight (270 g) in the QWBA studies. Patupilone distributed rapidly to most of the tissues including lung, liver, spleen, gut, brain, adipose, kidney, and testes, and concentration–time profiles were parallel to the blood concentration–time curve. For these tissues, patupilone distribution kinetics were described by perfusion rate-limited distribution models (or flow rate-limited model), assuming rapid membrane permeation and instantaneous partitioning equilibrium of drugs between a homogenous tissue and blood (Fig. 3b). The tissue-to-blood partitioning coefficient (K_p) was simply incorporated in perfusion-limited model to describe the distribution behavior between blood and the whole organ. Patupilone concentration profiles in the bone marrow and skin initially showed apparent distribution delays and were characterized by membrane permeability-limited models (diffusion-limited models) consisting of three sub-compartments that were divided into vascular, extracellular, and intracellular spaces (Fig. 3b) (9, 10) The parameter of K_p' was used to represent the instantaneous distribution between vascular and extracellular spaces, while a permeability-surface area product (PS_{tc}) was used to describe the slow permeation across the cell membrane. To date, patupilone has not been found to be a significant substrate for multidrug transporters, such as MDR1-type P-glycoprotein (ABCB1), the breast cancer resistance protein BCRP (ABCG2), and the multidrug resistance-associated proteins 1 through 5 (ABCC1-5) [36]. In the current study, transporter-mediated tissue permeation and distribution for patupilone were not considered.

Table 1 Physiological values of tissue volume and blood flow used in the generic GastroPlus rat PBPK model

Organ/tissues	Tissue type	Blood flow (mL/min)	Total volume (mL)
Lung	Perfusion rate limited	49.932	2.10
Spleen	Perfusion rate limited	0.600	0.60
Liver	Perfusion rate limited	13.800	10.30
Gut	Perfusion rate limited	7.500	
Adipose	Perfusion rate limited	0.402	10.00
Muscle	Perfusion rate limited	7.500	122.00
Heart	Perfusion rate limited	3.900	1.20
Brain	Perfusion rate limited	1.302	1.24
Kidney	Perfusion rate limited	9.198	3.70
Skin	Permeability rate limited	5.802	40.00, 0.38[a], 0.05[b], 0.57[c]
Testes	Perfusion rate limited	0.498	2.50
Bone marrow	Permeability rate limited	1.824	1.33, 0.1[a], 0.05[b], 0.85[c]
Arterial blood		49.932	5.60
Venous blood		49.932	11.30

[a] Fraction of vascular space in organs

[b] Fraction of interstitial space in organs

[c] Fraction of intracellular space in organs

Model equations

The mass balance for the rates of change in drug concentration in the venous (Eq. 1) and artery blood (Eq. 2) pool are [15]

$$V_{vb}\cdot\frac{dC_{vb}}{dt}=Q_{li}\frac{C_{li}}{K_{P_{li}}}+Q_{mu}\frac{C_{mu}}{K_{P_{mu}}}+Q_{bn}\frac{C_{bn}}{K_{P_{bn}}}+Q_{ad}\frac{C_{ad}}{K_{P_{ad}}}+Q_{br}\frac{C_{br}}{K_{P_r}}+Q_{ht}\frac{C_{ht}}{K_{P_{ht}}}+Q_{sk}\frac{C_{sk}}{K_{P_{sk}}}+Q_{ki}\frac{C_{ki}}{K_{P_{ki}}}+Q_{rep}\frac{C_{rep}}{K_{P_{rep}}}-Q_{lu}C_{ab} \quad (1)$$

$$V_{ab}\frac{dC_{ab}}{dt}=Q_{lu}\cdot\left(\frac{C_{lu}}{K_{P_{lu}}}-C_{ab}\right) \quad (2)$$

where V = organ volume, C = concentration, and Q = blood flow rate, vb = venous blood, ab = artery blood, li = liver, mu = muscle, bn = bone marrow, ad = adipose, br = brain, ht = heart, sk = skin, ki = kidney, rep = reproductive organ, and lu = lung.

The mass balance for noneliminating tissues where patupilone distribution followed perfusion rate-limited

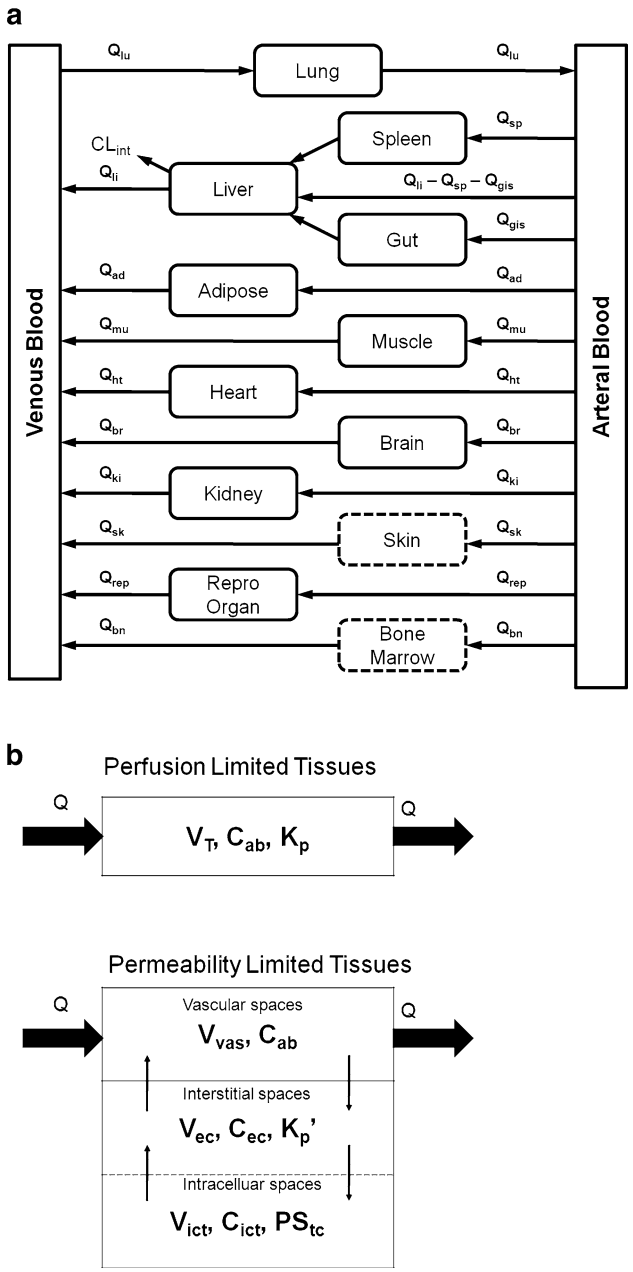

Fig. 3 **a** Schema of the GastroPlus v7.0 (Simulation Plus Inc., Lancaster, CA) generic disposition PBPK model for patupilone. Permeability-limited tissues models were represented in *dashed rectangular box*, while perfusion-limited tissue models were represented in *solid rectangular box*. The liver was assumed to be the only elimination tissue. **b** Model structures for perfusion-limited tissues and permeability-limited tissues

kinetics (adipose, heart, kidney, brain, muscle, spleen, and reproductive organ) was described by the following differential equation (Eq. 3)

$$V_{T_i}\frac{dC_{T_i}}{dt} = Q_{T_i}\cdot\left(C_{ab} - \frac{C_{T_i}}{K_{P_i}}\right) \quad (3)$$

where V_{T_i}, Q_{T_i}, C_{T_i}, K_{P_i} represent total organ volume, blood flow rate, tissue concentration, tissue-to-blood concentration partitioning ratio in tissue i.

For the lung, the mass balance was described as Eq. 4:

$$V_{lu}\frac{dC_{lu}}{dt} = Q_{lu}\cdot\left(C_{vb} - \frac{C_{lu}}{K_{P_{lu}}}\right) \quad (4)$$

For liver where patupilone was metabolized and eliminated, the mass balance was described as:

$$V_{li}\frac{dC_{li}}{dt} = Q_{sp}\cdot\frac{C_{sp}}{K_{P_{sp}}} + Q_{gis}\cdot\frac{C_{gis}}{K_{P_{gis}}} + (Q_{li} - Q_{sp} - Q_{gis})\cdot C_{ab} - Q_{li}\frac{C_{li}}{K_{p_{li}}} - CL_{int,u_{li}}\frac{C_{u_{li}}}{K_{p_{li}}} \quad (5)$$

where sp = spleen, gis = gut, while $CL_{int,u_{li}}$ and $C_{u_{li}}$ are unbound in vivo intrinsic clearance and concentration in liver. The relationship between observed system blood CL (CL_b) and $CL_{int,u}$ was described using the well-stirred model of clearance by Eq. 6:

$$CL_b = \frac{Q_H\cdot CL_{int,u_{li}}\cdot f_{up}}{Q_H + CL_{int,u_{li}}\cdot f_{up}} \quad (6)$$

where f_{up} is the fraction unbound in rat plasma of 0.3, and Q_H is the liver blood flow of 3.3 L/h/kg for rats. Then, the Eqs. 5 and 6 were rearranged to obtain:

$$V_{li}\frac{dC_{li}}{dt} = Q_{sp}\cdot\frac{C_{sp}}{K_{P_{sp}}} + Q_{gis}\cdot\frac{C_{gis}}{K_{P_{gis}}} + (Q_{li} - Q_{sp} - Q_{gis})\cdot C_{ab} - Q_{li}\frac{C_{li}}{K_{p_{li}}} - \frac{Q_H\cdot CL_b}{Q_H - CL_b}\cdot\frac{C_{u_{li}}}{K_{p_{li}}\cdot f_{up}} \quad (7)$$

For tissues where patupilone distribution was permeability rate limited (skin and bone marrow), the mass balance was described as:

$$\left(V_{ec} + \frac{V_{vas}}{K_p'}\right)\cdot\frac{dC_{ec}}{dt} = Q_T\left(C_{ab} - \frac{C_{ec}}{K_p'}\right) - PS_{tc}\cdot(C_{ec} - C_{ict}) \quad (8)$$

$$V_{ict}\cdot\frac{dC_{ict}}{dt} = PS_{tc}\cdot(C_{ec} - C_{ict}) \quad (9)$$

where ec, vas, ict, K_p', and PS_{tc} represented interstitial space, vascular space, intracellular space, partitioning coefficient between vascular and interstitial space, and permeability-surface area product for skin and bone marrow.

Parameter estimation

The physiological parameters (e.g., tissue volumes and blood flow rates) were obtained using the generic rat PBPK model of GastroPlus v7 (Table 1). All of compound-

dependent parameters (e.g., K_p, CL, PS_{tc}) of the PBPK models were obtained by fitting the data to all mass balance differential equations. The initial estimated value of rat liver $CL_{int,u}$ of patupilone was back-calculated from observed blood CL (0.33 L/h/kg) using Eq. 6 and was then incorporated in the PBPK model for data fitting. The drug distribution parameters (e.g., K_p, K_p', and PS_{tc}) were manually adjusted to obtain initial estimated values by visual inspection of the data fitting for each tissue. The initial estimated parameters were incorporated in the model and were further optimized based on weighted sum of squares of errors and a weighting factor of $1/\hat{y}^2$ (reciprocal of predicted concentration squared) using GastroPlus™ Optimization program. After convergence of model was achieved by the program, the curve-fitted PBPK parameters (e.g., K_p) were then generated. The final model was verified by the value of regression coefficient of the fit to the data, the Akaike Information Criterion (AIC), deviation of the predicted AUC_{0-72h} to the observed values.

Rat-to-human extrapolation of the PBPK parameters

The tissue-to-blood partitioning coefficient of unbound drug (K_{pu}) was defined as:

$$K_{Pu} = \frac{K_p \cdot R_{bp}}{f_{up}} \tag{10}$$

where K_p is the tissue-to-blood partition coefficient, and R_{bp} is blood-to-plasma partition ratio of the drug. Therefore, all rat K_p values estimated by the PBPK model was extrapolated to human with the assumption that human K_{pu} is equal to the rat K_{pu} based on Eq. 11 [11, 15].

$$K_{P(human)} = \frac{f_{up(human)}}{f_{up(rat)}} \cdot \frac{R_{bp(rat)}}{R_{bp(human)}} \cdot K_{P(rat)} \tag{11}$$

For the permeability-limited tissues, we conducted a scaling method for the parameter of PS_{tc} (L/h). Assuming that the permeability coefficient remains constant across species for a specific tissue, only the permeation surface area is considered to be scaled because the volume of tissue is different among species (Eq. 12). The ratio of tissue volume between humans and rats was currently used as the scaling factor for PS_{tc}.

$$PS_{tc(human)} = \frac{V_{T(human)}}{V_{T(rat)}} \cdot PS_{tc(rat)} \tag{12}$$

where V_T stands for the tissue volume according to default physiological volume in GastroPlus v7 PBPK model.

For the prediction of system clearance in human, it was assumed that liver metabolism was the only eliminating pathway for humans, and renal and biliary excretion had almost no contribution to the systemic clearance. The in vitro–in vivo extrapolation (IVIVE) method was used to calculate the in vivo clearance scaled from the in vitro metabolism kinetics determined by microsomal incubation study. The microsomal incubation data were fitted using a Michaelis–Menten kinetics model with calculated values of V_{max} and K_m as described previously. Then, unbound in vitro clearance in human liver microsome ($CL_{int,u,in\ vitro}$) was calculated as follows:

$$CL_{int,u,in\ vitro} = \frac{V_{max}}{K_m \cdot f_{u,mic}} \tag{13}$$

where $f_{u,mic}$ is the unbound fraction of patupilone in human liver microsomal incubation. The value of $f_{u,mic}$ was estimated using the equation developed by Kilford et al. [17] as:

$$f_{u,mic} = [C_{mic} \times 10^{0.072 \cdot (\mathrm{Log}P|D)^2 + 0.067 \cdot \mathrm{Log}P|D - 1.126} + 1]^{-1} \tag{14}$$

where log P or log D represents either log $D_{pH=7.4}$ (for acidic and neutral drugs) or log P (for bases) as descriptors for drug lipophilicity, and C_{mic} represents the protein concentration in the microsome incubation. The obtained $CL_{int,u,in\ vitro}$ was scaled to in vivo human hepatic intrinsic clearance ($CL_{int,u_{li}}$) by the scaling factors based on empirical physiological parameters as [20]:

$$CL_{int,u,li} = CL_{int,u,in\ vitro} \cdot X \cdot Y \tag{15}$$

where X is 48.8 mg microsomal protein/g liver, and Y is 25.7 g liver weight/kg body weight in humans. The in vivo CL_H was thus calculated using a well-stirred model of hepatic clearance described by Eq. 6, where the f_{up} for human is 0.3 and the human hepatic blood flow (Q_H) is 1.24 L/h/kg.

Human PK profile prediction using a PBPK approach

The schema for the human PBPK model is analogous to the rat model. The parameters of K_p and PS_{tc} were calculated by the scaling method described in the previous section as the model input. Population-dependent physiological parameters in human PBPK models were obtained using the Population Estimates for Age-Related Physiology™ (PEAR) module in GastroPlus v7, where the generic parameters (e.g., tissue volume, perfusion rate) for Caucasian and Japanese patients were based on the National Health and Nutrition Examination Survey and the data published by Ogiu et al. [25], respectively. The population-specific information, such as age, gender, ethics, and body weight, are customized according to the patient information in the PEAR module. In turn, the related tissue physiological values, including tissue volume, tissue

perfusion rates, and tissue densities, were automatically generated by the PEAR module according to the user-specified population data. The current clinical trials for patupilone included the population of both Caucasian and Japanese patients. Simulations were performed in 9 dose cohorts ($n \geq 2$ in each cohort), including 3 groups of Caucasian males, 3 groups of Caucasian females, 2 groups of Japanese males, and one group of Japanese female. The population data in each dose cohort were incorporated in the PEAR module to develop a corresponding PBPK model.

Model assessment of the human pharmacokinetics prediction

The simulated human PK profiles were compared with the observed data for each dose cohort in both studies. Non-compartmental analysis was used to calculate pharmacokinetic parameters for predicted and observed human pharmacokinetic profiles using the WinNonlin Pheonix v6.1. The accuracy of prediction for pharmacokinetic parameters (e.g., CL, V_{ss}, $t_{1/2}$) was evaluated by the criteria of the fold error (FE), which has been published previously (Eq. 16) [10, 11, 15, 24, 29]. If the predicted values of the major pharmacokinetic parameters (e.g., CL, V_{ss}, AUC, $t_{1/2}$) fall within twofold of the observed values (FE $\leq$ 2), the model is considered to have high accuracy of prediction.

$$\mathrm{FE} = 10^{\left|\log\left(\frac{\text{Predicted}}{\text{Observed}}\right)\right|}. \quad (16)$$

Results

Enzyme kinetics of patupilone metabolism in human liver microsomes

The apparent enzyme kinetic parameters for the rate of depletion of ^{14}C-patupilone metabolites in pooled human liver microsomes were determined at 0.25–300 μM substrate concentration. The percentage of patupilone metabolized in the incubation ranged from 10 to 20 % at all substrate concentrations. The depletion rate of patupilone in human liver microsome followed a monophasic Michaelis–Menten kinetics with an apparent maximal velocity of the metabolism (V_{max}) of 681 pmol/min/mg protein and a Michaelis constant (K_m) of 223 μM (Fig. 4a).

Disposition of patupilone and total radioactivity in rats

The blood and total radioactivity concentration–time profile were presented in Fig. 4b. Concentration–time curves for radioactivity and patupilone were parallel throughout the entire observation period. Radioactivity and parent compound concentration in blood were detected for 72 h after dosing but, thereafter, were below the limit of quantification of conventional LSC and LC–MS/MS.

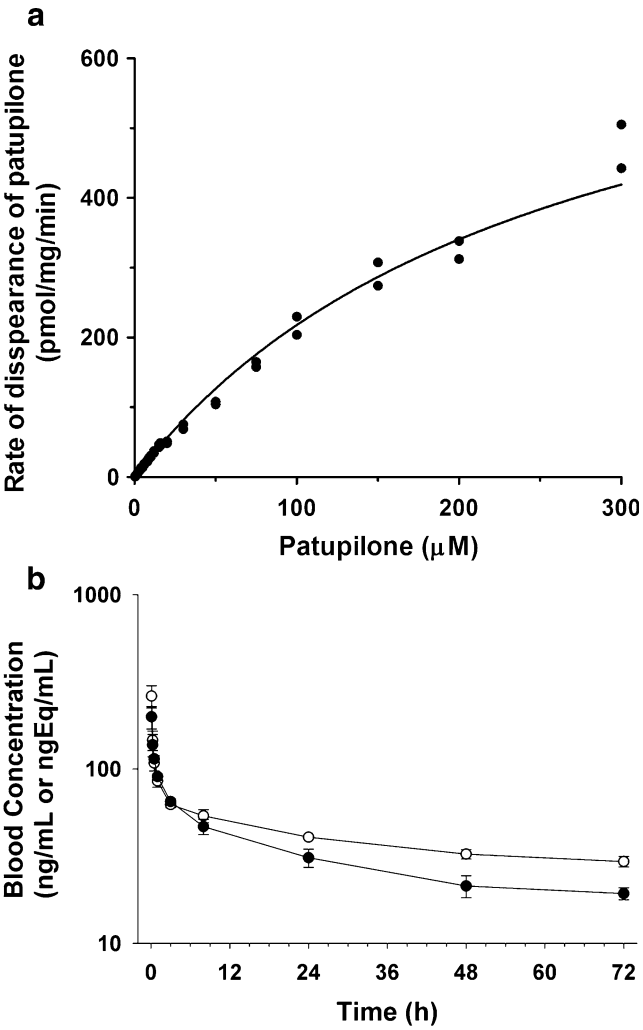

Fig. 4 **a** Kinetics of patupilone metabolism in pooled human liver microsomes. Experimental data were fitted using a Michaelis–Menten kinetics model. **b** Concentration–time profiles for parent drug of patupilone (*solid circles*) and total radioactivity (*opened circles*) in rat blood at a 1.2 mg/kg of intravenous dose

The pharmacokinetic parameters for radioactivity and patupilone in blood were calculated from noncompartmental analysis and were summarized in Table 2. The estimated terminal half-lives of patupilone and radioactivity were 47 and 73 h, respectively. Approximately, 78 % of total blood radioactivity was accounted for unchanged patupilone (AUC_{0-72h}), indicating low exposure to metabolites in rats. The observed $AUC_{(0-72h)}$ values of patupilone acid, 1,16-diol-patupilone acid, and sum of the other trace metabolites in blood accounted for 6.1, 0.55, and 7.2 % of the AUC value of total radioactivity, respectively. Following an intravenous administration (1.2 mg/kg) of ^{14}C-patupilone, the systemic blood clearance (CL_b) of patupilone was 0.33 ± 0.04 L/h/kg, suggesting patupilone

Table 2 Pharmacokinetic parameters for the total patupilone-related radioactivity and intact patupilone parent drug

Parameters	Patupilone	Total radioactivity
Dose (mg/kg)	1.2	1.2
AUC^{∞} (μM h)	7.1 ± 0.7	12.0 ± 1.4
CL_b (L/h/kg)	0.33 ± 0.04	0.19 ± 0.02
V_{ss} (L/kg)	21.1 ± 1.7	22.9 ± 4.7
$t_{1/2}$ (h)	47.0 ± 10.1	73.4 ± 12.1

Estimates are presented as mean values ± standard deviation (*ND* not determined)

is a drug with low hepatic extraction ratio (~10 % of the hepatic blood flow rate of 3.3 L/h/kg). The volume of distribution of patupilone was 21.1 ± 1.7 L/kg, which was greater than the total body water. The total radioactivity and patupilone in blood declined rapidly within 3 h and exhibited a slower decline up to 72 h (Fig. 4b). Compared to the mean radioactivity concentrations, the mean concentration of patupilone in blood was almost identical from 0.33 to 6 h post-dose but was slightly lower at 0.083 h and after 6 h. The radioactivity excreted in urine, bile, and feces accounted for 4.2, 51.4, and 2.3 % of the dose, respectively. In urine and feces, only 0.03 and 0.12 % of intact patupilone was recovered. The mass balance recovery from all of excreta and cage wash was less than 70 % for 72 h after dose, and the rest of radioactivity (~32 %) was recovered in carcass, suggesting that patupilone has a high tissue binding affinity. In bile, patupilone was hardly detected. Its metabolites accounted for nearly all of radiolabeled components recovered, indicating an extensive biliary excretion of the metabolites but not the parent compound.

The tissue distribution of patupilone was determined by quantitative whole-body auto-radioluminography (QWBA). The radioactivities in most of the tissues were higher than that of the blood radioactivity determined in the pharmacokinetic disposition study (group A) at all corresponding time points. The radioactivity concentrations in all tissues declined in a biphasic manner with an initial rapid phase and a very slow elimination except in skin and bone marrow where concentration first increased gradually until 8 h post-dose and then declined slowly (Fig. 2a). The overall radioactivity exposure ($AUC_{0–72h}$) was highest in spleen, lung, and kidney, whereas it was lowest in adipose, testes, and brain.

Pharmacokinetics in human

The pharmacokinetic parameters of patupilone were calculated by noncompartmental analysis using WinNonlin Phoenix v6.1. After the intravenous infusion, patupilone concentrations declined rapidly followed by a prolonged terminal phase with a half-life of approximately 4.5 days. The average blood clearance of patupilone was approximately 9.0 L/h, which is ~10 % of hepatic blood flow rate (~90 L/h). A large volume of distribution (>14 L/kg) was consistent with extensive tissue distribution of patupilone reported in the preclinical studies. Renal excretion of unchanged patupilone in 48 h was 0.05 % of total dose infused, indicating that the renal excretion was a minor route of elimination.

Table 3 Estimated parameters and goodness-of-fit analysis of patupilone PBPK model in rats

Organ/tissues	K_p	PS_{tc} (L/h)	Regression coefficient (R^2)	Deviation of prediction on $AUC_{0–72h}$ (%)[c]
Lung	29		0.99	− 6.2
Spleen	85		0.78	11.5
Liver[a]	35.0		0.90	11.5
Adipose	2.70		0.84	13.5
Muscle	24.9		0.90	20.2
Heart	19.6		0.78	1.5
Brain	4.20		0.88	−26.5
Kidney	46.3		0.73	7.9
Skin[b]	1.2	0.295	0.86	16.7
Testes	2.20		0.93	0.54
Bone marrow[b]	2.09	0.02	0.98	0.40
Blood			0.95	5.1

[a] Hepatic blood intrinsic clearance in the rat PBPK model was fitted as 0.315 L/h/kg

[b] Skin and bone marrow were modeled as a permeability-limited tissue

[c] Deviation (%) was calculated as (Predicted $AUC_{0–72h}$/Observed $AUC_{0–72h}$ − 1) × 100

PBPK model development in rats

The tissue concentration–time profiles were fitted into the rat PBPK model using the optimization tools of GastroPlus v7. The obtained PBPK parameters, including K_p, hepatic clearance (CL), and PS_{tc} (for permeability-limited tissues), are described in Table 3. Simulated tissue concentration–time profiles of patupilone were compared with the observed tissue concentrations (Fig. 5). The simulated results yielded a satisfactory agreement with the observed tissue concentrations, suggesting successful data fitting and modeling for rat data. Patupilone concentration versus time curves for perfusion rate-limited organs (heart, lung, spleen, adipose, muscle, liver, kidney, adipose, and brain) declined in parallel with plasma concentration, and overall, the model was able to capture the overall behavior of the concentration profile very well with regression coefficient of the fitting greater than 0.73. The estimated partition

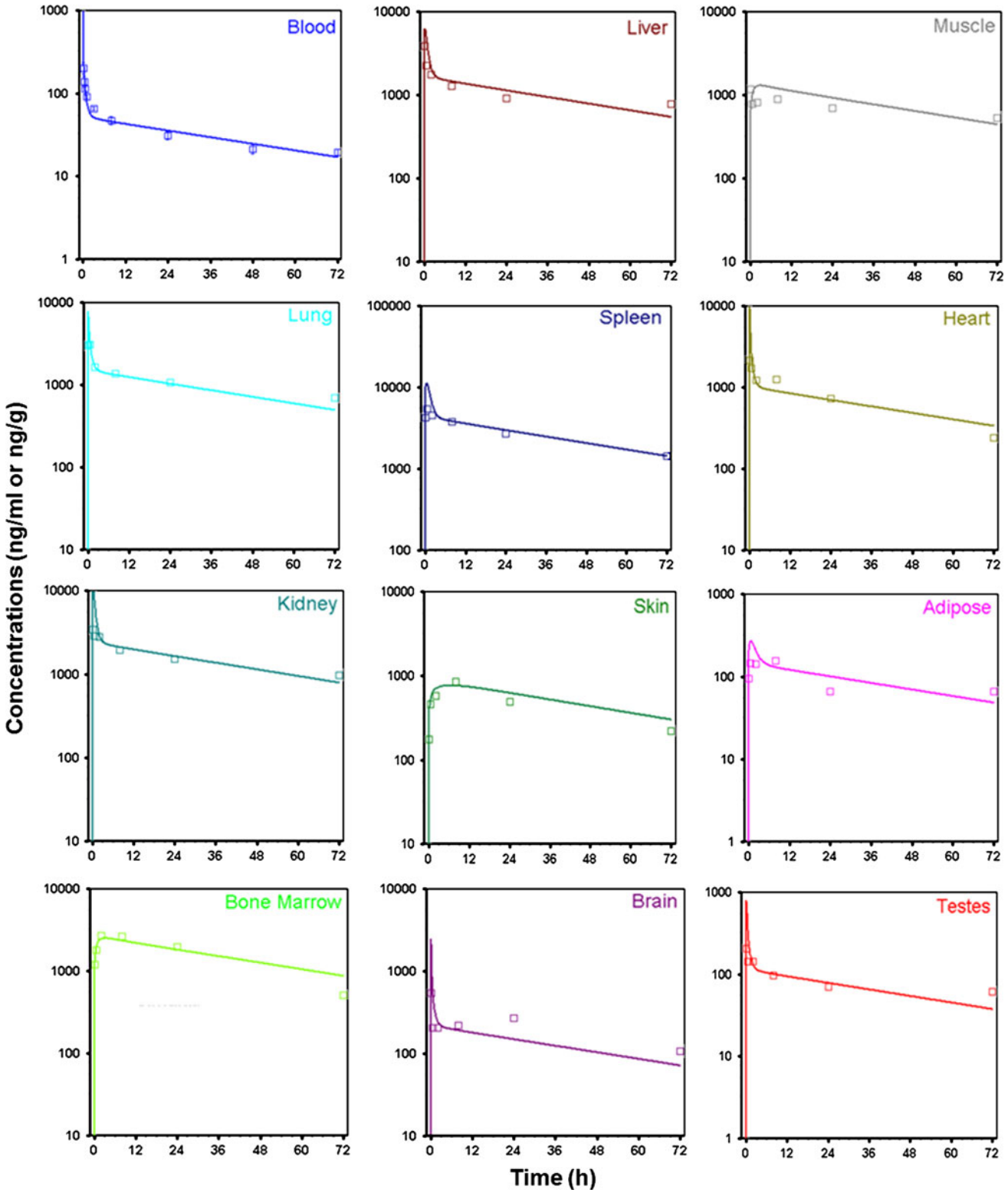

Fig. 5 Data fitting of the rat PBPK model for blood, liver, muscle, lung, spleen, heart, kidney, skin, adipose, bone marrow, brain, and testes after a single intravenous dose of 1.2 mg/kg in rats. Predicted values were represented as *solid curves*, and observed tissue concentrations were shown in *opened squares*

coefficient for all of the perfusion-limited tissue varied extensively from 2.2 (testes) to 85 (spleen). Except for adipose tissues, brain, and testes, the tissue-to-blood partition coefficients for all of the perfusion rate-limited organs were greater than 10, suggesting significant tissue binding. Patupilone concentration–time profile in skin and bone marrow exhibited a delayed distribution and was well fitted by the permeability rate-limited tissue model with regression coefficients of 0.86 and 0.98, respectively. Overall, the model achieved a reasonable AIC value of 78.1, and the predicted tissue exposures described by AUC_{0-72h} were both within ±27 % deviation of those observed in the QWBA data for all the tissues (Table 3). The resulting parameters from the rat PBPK model were then scaled to the human.

Human PBPK modeling

The human physiological values, including tissue volume and tissue perfusion rates, were automatically generated based on input of the patient information in each dose cohort using GastroPlus build-in PEAR module. Human K_p values were scaled from rat K_p with the correction f_{up} and R_{bp}. The unbound fraction of plasma protein binding and blood-to-plasma partition ratio was 0.30, 0.30 and 1.8, 0.91 for rats and humans, respectively. Therefore, the human K_p was about 2-folder higher than rat K_p according to Eq. 10. In addition, since tissue distribution data were not available for the reproductive organ for female rats, the value of rat testes K_p was used to extrapolate the K_p of human reproductive organ for both male and female patients. For permeability-limited tissues, the parameter of PStc in humans was higher than that in rats because tissue volumes are much higher. The human clearance was estimated by an IVIVE method using kinetics data measured by the human microsomal incubation studies [31]. The metabolism of patupilone in human liver microsome followed monophasic Michaelis–Menten kinetics (Fig. 4a). The estimated unbound fraction of patupilone in human liver microsomes incubation ($f_{u,mic}$) was 0.62 using Eq. 14 [2]. Therefore, the unbound in vitro clearance ($CL_{in\ vitro}$) was 4.9×10^{-3} mL/min/mg protein calculated from estimated Michaelis–Menten parameters (V_{max} and K_m) using Eq. 13. Then, in vivo human hepatic intrinsic clearance ($CL_{int,u_{li}}$) was scaled to 6.14 mL/min/kg (0.37 L/h/kg) using the empirical human physiological parameters (Eq. 15) [20] and was incorporated into human PBPK model for simulation. The human CL_H was then predicted as 1.70 mL/min/kg (0.10 L/h/kg) using hepatic well-stirred model (Eq. 6) [20]. According to the mean body weight of the patients in each dose cohort (ranged: 54–87 kg), the human CL ranged from 5.5 to 8.9 L/h. The extrapolated human PBPK parameters, including K_p, tissue volume-normalized PS_{tc} (unit: 1/h), and CL, were summarized in Table 4.

Table 4 Extrapolated parameters of patupilone used in the human PBPK model

Parameters	Unit	Extrapolated values		
K_p	N/A	Lung: 57.4	Brain: 8.31	Kidney: 91.6
		Liver: 69.2	Heart: 38.8	Spleen: 168.13
		Muscle: 49.3	Adipose: 5.34	Skin: 2.37
		Bone marrow: 4.10	Reproductive organ: 4.35	
PS_{tc}	L/h/organ volume	Skin: 7.38	Bone marrow: 15.7	
CL	L/h/kg		0.10	

Model assessment

The PBPK model simulation was conducted using 9 groups of human intravenous pharmacokinetic data from two separate Phase I dose-escalation clinical trials where Caucasian (6 groups) and Japanese patients (3 groups) were selected, respectively. The correlations between the observed and predicted human pharmacokinetic profiles for each group are presented in Fig. 6. Overall, the observed blood concentrations were in good agreement with the predicted curves. The predicted human AUC, $t_{1/2}$, V_{ss}, and CL for all dose cohorts fell within 2.1-fold of those observed (Tables 5, 6), indicating that the current human PBPK model provided high prediction accuracy. The prediction accuracy of the pharmacokinetic parameters showed no apparent significant differences across ethnic and gender groups.

Discussion

The successful development of new drug candidates with both efficacious and safe systemic exposures requires accurate prediction of human pharmacokinetic (PK) profiles to assist various aspects of clinical trials, including choosing suitable dosing regimen, assessing risks of toxicity, predicting potential individual variability, and saving research funds and time [13]. Two most common approaches for human PK predictions are allometric scaling and physiologically based pharmacokinetic (PBPK) modeling. Allometric scaling is an established prediction approach by extrapolation of PK parameters based on their corresponding body weights [16, 31]. PBPK modeling is a mechanism-based approach which incorporates physiological and anatomical factors as well as the physico–chemical properties of

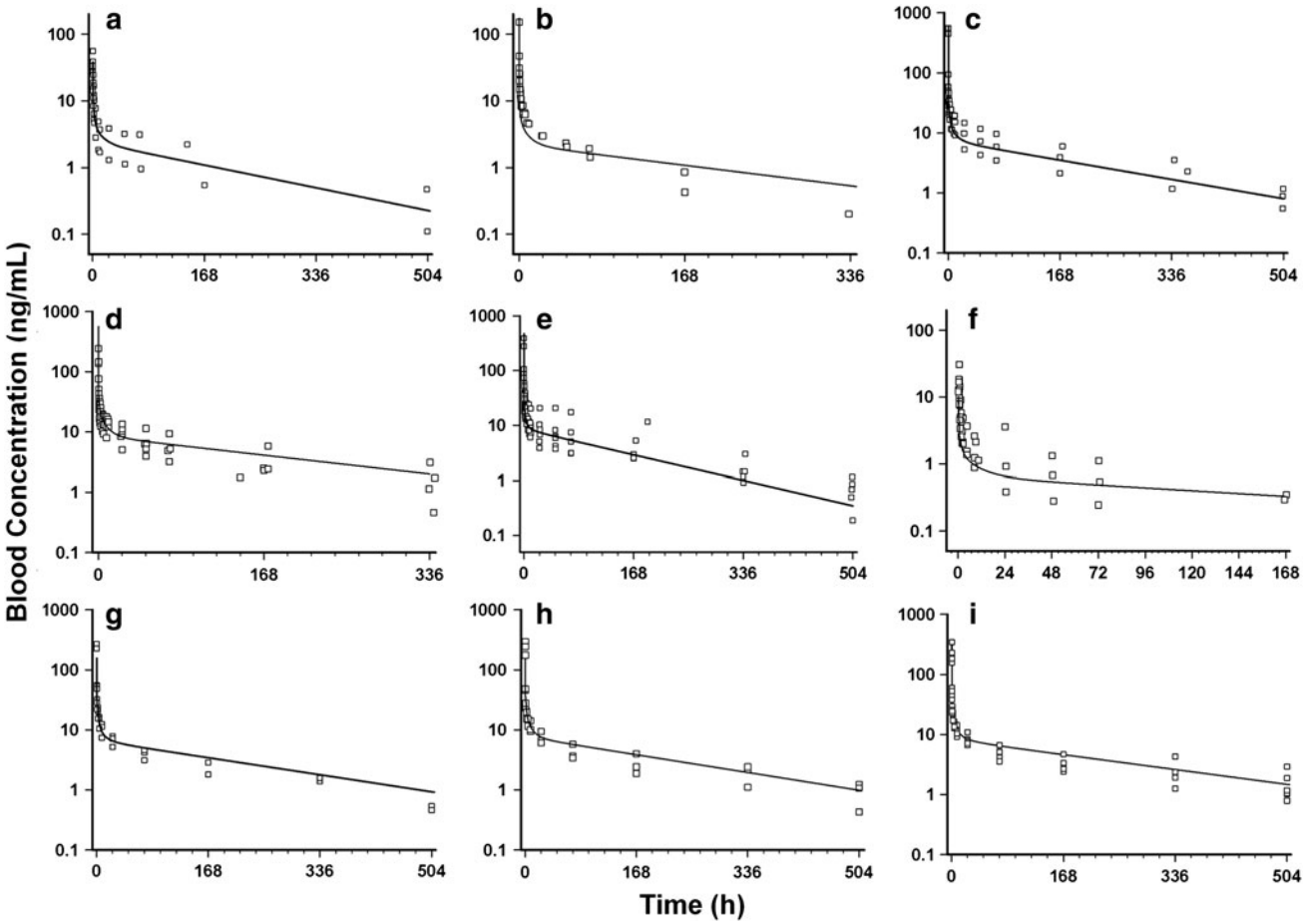

Fig. 6 Predicted and observed human blood concentration–time profiles using method after an intravenous dose of patupilone of **a** 2.4 mg/m^2 in American male patients, **b** 2.4 mg/m^2 in American female patients, **c** 8 mg/m^2 in American male patients, **d** 8 mg/m^2 in American female patients, **e** 6 mg/m^2 in American male patients, **f** 0.75 mg/m^2 in American female patients, **g** 7.5 mg/m^2 in Japanese male patients, **h** 7.5 mg/m^2 in Japanese female patients, or **i** 10 mg/m^2 in Japanese male patients. Predicted values were represented as *solid curves*, and observed data from individual patients were shown in *opened squares*

Table 5 Predicted and observed human pharmacokinetic parameters in Caucasian and Japanese patients receiving a single intravenous dose of patupilone

Gender	Ethnics	Dose (mg/m^2)	V_{ss} (L)		CL (L/h)		$AUC_{0\text{-last}}$ (h*ng/mL)		$t_{1/2}$ (h)	
			OBS	PRE	OBS	PRE	OBS	PRE	OBS	PRE
M	Caucasian	8	1,575	1,635	8.20	8.90	2,125	1,646	158	127
F	Caucasian	8	954	1,052	8.49	5.90	1,700	1,660	97.65	124
M	Caucasian	2.4	1,415	1,495	8.70	8.06	652	520	140	128
F	Caucasian	2.4	730	1,357	9.95	7.43	414	447	67	127
M	Caucasian	6	1,360	922	6.43	8.17	1,870	1,367	160	78
F	Caucasian	0.75	940	1,418	10.84	8.04	136	93	74.7	132
M	Japanese	10	1,870	1,576	8.08	6.52	1,620	2,197	262	168
M	Japanese	7.5	1,900	1,459	10.36	7.50	1,210	1,621	149	134
F	Japanese	7.5	1,590	1,005	7.08	5.52	1,430	1,805	191	125

OBS observed values, *PRE* predicted values

a compound into a mathematical model consisting of tissue mass balance differential equations. In the past, PBPK models were rarely used in early drug development due to intensive experimental data input requirements along with mathematical complexity. Recently, due to the availability of the tissue composition equations developed for the

Table 6 Fold errors for predicted PK parameters in Caucasian and Japanese patients

Ethnics	Gender	Dose (mg/m^2)	mL (FE)			
			V_{ss}	CL	$AUC_{0\text{-last}}$	$t_{1/2}$
Caucasian	M	8	1.04	1.09	1.29	1.24
	F	8	1.10	1.44	1.02	1.27
	M	2.4	1.06	1.08	1.25	1.09
	F	2.4	1.86	1.34	1.08	1.90
	M	6	1.48	1.27	1.37	2.05
	F	0.75	1.51	1.35	1.46	1.77
	Mean ± SD fold error		1.34 ± 0.33	1.26 ± 0.15	1.24 ± 0.107	1.55 ± 0.40
Japanese	M	10	1.19	1.24	1.36	1.56
	M	7.5	1.30	1.38	1.34	1.11
	F	7.5	1.58	1.28	1.26	1.53
	Mean ± SD fold error		1.36 ± 0.20	1.30 ± 0.07	1.32 ± 0.05	1.40 ± 0.25
Mean ± SD fold error for all group			1.35 ± 0.28	1.27 ± 0.12	1.27 ± 0.14	1.50 ± 0.35

prediction of in vivo tissue-to-plasma partitioning coefficient (K_p) [29, 32, 33], the application of PBPK modeling has become more popular as illustrated by an accelerating number of scientific publications during the past decade [34]. Recent published reports demonstrated the novel strategies of PBPK modeling using the tissue composition equations developed by Poulin or Rodgers et al. and also assessed the prediction accuracy of such modeling approaches using a retrospective analysis for sets of compounds that were brought into clinical development [10, 11, 14, 15]. However, poor prediction accuracy of human volume of distribution (V_d) has been reported for more than 50 % of the tested compounds [11, 15, 28]. Better prediction accuracy of human V_d was observed with experimentally determined K_p from rodents (e.g., rats and mice) and further extrapolated to estimate human K_p with the correction of plasma protein binding [11]. According to an industrial PBPK prediction strategy decision tree, incorporation of rat tissue distribution data into PBPK models is an alternative approach when tissue composition equation methods are unsuccessful [15].

In recent years, the use of tissue distribution data has experienced significant changes [26, 32–34]. The conventional approach of preselected tissue dissection was gradually replaced by quantitative whole-body autoradiography (QWBA) during the past decade because QWBA data can provide more comprehensive evaluations of the disposition of drug-related radioactivity than the laborious preselected tissue dissection approach [9, 27]. Incorporation of QWBA data in the PBPK may enhance the confidence for the prediction of human V_d. However, such attempts may lead to inaccurate prediction on K_p because QWBA studies provide the total radioactivity data that combine the concentrations of both intact parent compound and its metabolites. Therefore, when QWBA tissue data are used as the input for PBPK models, caution must be taken to consider the radioactivity concentration contribution by the metabolites, especially for moderately to highly metabolized compounds [11, 15]. Patupilone is exclusively eliminated by metabolism in rats and humans with a relative low metabolic clearance (~10 % of liver blood flow). Unchanged patupilone in its lactone form was observed as the major circulation component in rat blood and is much more lipophilic than its metabolites that were mostly derivatives of acids. For noneliminating organs, it can be safely assumed that metabolites of patupilone were significantly less permeable to cell membranes and have much lower systemic exposures than the parent compound. For the eliminating organ of liver, while it can be expected that the permeability is too low for metabolites to diffuse out of hepatocytes, we assumed that metabolites formed in hepatocytes did not accumulate in liver due to the following two reasons: (1) the radioactivity recovered in bile only accounted for the metabolites of patupilone, suggesting that metabolites of patupilone in hepatocytes were eliminated through active secretion possibly mediated by the uptake of biliary transporters; (2) biliary excretion was the predominant elimination pathway for the radioactivity, indicating rapid clearances of metabolites from liver. Overall, the QWBA radioactivity data can be directly used as the parent drug tissue concentration for rat PBPK model. This assumption was further verified by QWBA radioactivity concentration–time curves in brain, muscle, and liver, which are nearly identical with the corresponding patupilone tissue concentration–time curves measured by LC–MS/MS [22] (Fig. 2).

In vivo, patupilone is a potent inhibitor of tumor growth in various multidrug-resistant human tumor models mediated by P-gp, β-tubulin mutations, or other mechanisms. Efficacy was achieved at dose levels (up to 10 mg/m^2) that were well tolerated, suggesting that patupilone could be an appropriate treatment for multidrug-resistant tumors

including tumors refractory to taxanes [18, 21–23]. Efficacy of patupilone has been evaluated in a number of indications in clinical trials, including colorecatal, prostate, nonsmall cell lung cancer, and ovarian cancer. Few publications have investigated epothilones distribution in tissues; however, due to the promising inhibitory effects of patupilone against many types of tumors, the dispositions of patupilone in human tissue have currently been of interest. To characterize the antitumor activity of patupilone in various organs, a PBPK/PD model is required to predict the tissue concentrations to link the tissue concentration to efficacy. To our knowledge, no prior attempts have been made to model the disposition of epothilones using a "whole-body" PBPK model in rats and humans. Here, a rat PBPK model was developed to fit to tissue concentration–time profiles and subsequently obtain tissue distribution parameters of K_p and PS_{tc}. The rat model was used as the basis for developing a human patupilone PBPK model. The values of rat K_p and PS_{tc} were scaled to human for the estimation of V_d and the projection of clinical pharmacokinetic profiles using Eqs. 11 and 12. The scaling of K_p values to human assumed that the unbound partition coefficient (K_{pu}) is the same between rats and humans, while the differences of K_p between species were contributed by the differences of plasma protein binding and blood-to-plasma partition ratio. The scaling of PS_{tc} values assumes that the apparent permeation rate was identical between rats and humans for a specific tissue and the ratio of tissue volume between species needed to be scaled. In other words, the values of tissue volume-normalized PS_{tc} are equal between human and rats.

The rat model successfully described the tissue disposition of patupilone in nearly all the tissues as well as the blood pharmacokinetics of the drug. In most of the tissues, patupilone distribution kinetics can be described by simple perfusion-limited model because the concentration profiles in these tissues were parallel to the blood concentration profile. On the other hand, patupilone concentrations in bone marrow and skin showed initial distribution delays that were not well described by the perfusion-limited tissue model. Instead, such behaviors were characterized by membrane permeability-limited models (diffusion-limited models) consisting of three sub-compartments. The radioactivities in most tissues were higher than in blood determined in pharmacokinetic disposition studies at all corresponding time points. It was believed that patupilone highly bound to tissues in vivo, which is in accordance with the finding that the binding affinity to cellular microtubules of patupilone was several times higher than that of paclitaxel [6, 30]. Patupilone can pass the blood–brain or blood–testes diffusion barrier in rats although the brain and testes concentrations in rats were lower than those in other tissues. Elimination from brain and testes was slow, which is consistent with the fact that the efflux of the drug appeared not to associate with multidrug-resistant transporters that are richly expressed in brain and testes. Similarly, it is safe to assume that patupilone was able to cross the blood–ovary barrier and retains in the tissue for long time although tissue distribution data were not available for the reproductive organ for female rats.

The human physiological values used in the PBPK model were generated by the PEAR module of GastroPlus™ v7. The PEAR-based PBPK model reflected the individual variability of physiology by incorporating the factors of ethnic groups, age, gender, and body weight that allowed more reliable simulation for population pharmacokinetic data. For the prediction of human CL in PBPK models, IVIVE is a commonly used method [31]. The IVIVE method successfully predicted the CL within 1.45-fold of the observed value; however, it was noted the overall prediction bias was slightly toward underestimation of the observed value (Table 5). The underestimation may be caused by the reason that carboxyl-esterases exist not only in microsomes but also in other intracellular organelles (e.g., mitochondria) and fluids (e.g., cytosols). Therefore, the intrinsic clearance calculated from in vitro microsomal incubation will be slightly lower than the actual observed values. Overall, the extrapolated human K_p in the PBPK model accurately predicted the V_{ss} in all clinical dose cohorts with an average prediction error less than 1.35. The deviation of prediction for terminal $t_{1/2}$ was slightly larger than those for V_{ss} and CL. It was noted that the prediction accuracy was relatively poor for $t_{1/2}$ when the deviation of predicted V_{ss} and CL was relatively larger. Therefore, our finding indicated that accurate predictions of in vivo terminal $t_{1/2}$ depend on the prediction accuracy of CL and V_{ss}, which is also in agreement with previous reports [11].

In summary, the distribution of patupilone in rats was well described using a PBPK model based on tissue distribution data generated by QWBA combined with metabolism data. The PBPK model successfully characterized the blood pharmacokinetics of patupilone in cancer patients. The present PBPK modeling work has been structured to be consistent with known physiology and cellular processes of patupilone disposition. This model may aid in the prediction of patupilone disposition and establish the concentration and efficacy relationship within several drug targets that are currently under development. In addition, the paper outlined an interesting approach to extend the utility of PBPK model to predict pharmacokinetics using QWBA data when in silico predictions are insufficient.

Acknowledgments We thank Dr. Hilmar Schiller for conducting in vitro metabolism study and Dr. Swati Dumitras, Dr. Markus Zollinger, and Corinne Emotte for contributions in animal studies.

Conflict of interest None.

References

1. Altmann KH, Wartmann M, O'Reilly T (2000) Epothilones and related structures—a new class of microtubule inhibitors with potent in vivo antitumor activity. Biochim Biophys Acta 1470: M79–M91
2. Austin RP, Barton P, Cockroft SL, Wenlock MC, Riley RJ (2002) The influence of nonspecific microsomal binding on apparent intrinsic clearance, and its prediction from physicochemical properties. Drug Metab Dispos 30:1497–1503
3. Beardsley EK, Saad F, Eigl B, Venner P, Hotte S, Winquist E, Ko YJ, Sridhar SS, Chi KN (2009) A phase II study of patupilone in patients (pts) with metastatic castration-resistant prostate cancer (CRPC) who have progressed after docetaxel. J Clin Oncol 27:1–6
4. Bollag DM, McQueney PA, Zhu J, Hensens O, Koupal L, Liesch J, Goetz M, Lazarides E, Woods CM (1995) Epothilones, a new class of microtubule-stabilizing agents with a taxol-like mechanism of action. Cancer Res 55:2325–2333
5. Brezniceanu LM, Deroussent A, Gu H, Mangold JB, Schiller H, Gross G, Cresteil T (2008) Oxidative metabolism of epothilones A and B (Patupilone) by cytochromes P450: involvement of CYP3A and CYP2C. Open Drug Metab J 2:14–23
6. Buey RM, Diaz JF, Andreu JM, O'Brate A, Giannakakou P, Nicolaou KC, Sasmal PK, Ritzen A, Namoto K (2004) Interaction of epothilone analogs with the paclitaxel binding site: Relationship between binding affinity, microtubule stabilization, and cytotoxicity. Chem Biol 11:225–236
7. Casado E, Tabernero J, Melichar B, Bridgewater J, Bennouna J, Delord J, Sopala M, Sklenar I, Cheung W, Johri A (2006) Patupilone in chemotherapy-pretreated patients with advanced colorectal cancer (CRC) receiving nutritional support and intensive diarrhea management: a phase I multicenter trial. J Clin Oncol. 2006 ASCO annual meeting proceedings part I, vol 24, no 18S (June 20 Supplement), 3593 [abstract]
8. Chi KN, Beardsley E, Eigl B, Venner P, Hotte SJ, Winquist E, Ko YJ, Saad F (2008) A phase 2 study of patupilone in patients with metastatic hormone refractory prostate cancer (Hrpc) who have progressed after docetaxel. J Clin Oncol. 2008 ASCO annual meetings, vol 26, (May 20 Supplement), 5166 [abstract]
9. Coe RA (2000) Quantitative whole-body autoradiography. Regul Toxicol Pharmacol 31:S1–S3
10. De Buck SS, Sinha VK, Fenu LA, Gilissen RA, Mackie CE, Nijsen MJ (2007) The prediction of drug metabolism, tissue distribution, and bioavailability of 50 structurally diverse compounds in rat using mechanism-based absorption, distribution, and metabolism prediction tools. Drug Metab Dispos 35:649–659
11. De Buck SS, Sinha VK, Fenu LA, Nijsen MJ, Mackie CE, Gilissen RAHJ (2007) Prediction of human pharmacokinetics using physiologically based modeling: a retrospective analysis of 26 clinically tested drugs. Drug Metab Dispos 35:1766–1780
12. Gore M, Forster M, Kaye S, Oza A, Sklenar I, Johri A, Cheung W, Zaknoen S (2007) A phase lb and pharmacokinetic trial of patupilone combined with carboplatin in patients with advanced cancer. Clin Cancer Res 13:4178–4184
13. Heimbach T, Lakshminarayana SB, Hu W, He H (2009) Practical anticipation of human efficacious doses and pharmacokinetics using in vitro and preclinical in vivo data. AAPS J 11:602–614
14. Jones HM, Gardner IB, Watson KJ (2009) Modelling and PBPK simulation in drug discovery. AAPS J 11:155–166
15. Jones HM, Parrott N, Jorga K, Lave T (2006) A novel strategy for physiologically based predictions of human pharmacokinetics. Clin Pharmacokinet 45:511–542
16. Jones RD, Jones HM, Rowland M, Gibson CR, Yates JW, Chien JY, Ring BJ, Adkison KK, Ku MS, He H, Vuppugalla R, Marathe P, Fischer V, Dutta S, Sinha VK, Bjornsson T, Lave T, Poulin P (2011) PhRMA CPCDC initiative on predictive models of human pharmacokinetics, part 2: comparative assessment of prediction methods of human volume of distribution. J Pharm Sci 100:4074–4084
17. Kilford PJ, Gertz M, Houston JB, Galetin A (2008) Hepatocellular binding of drugs: correction for unbound fraction in hepatocyte incubations using microsomal binding or drug lipophilicity data. Drug Metab Dispos 36:1194–1197
18. McSheehy R, O'Reilly MT, Wartmann M, Maira M, Allegrini P, Brueggen J (2007) Patupilone, the novel microtubule stabilizer (MTS), retains activity against human colon tumour cells overexpressing P-gp in vitro and in vivo; comparison with other MTS. EJC Suppl 14th European Cancer Conference (ECCO 14), vol 5, p 63, 323 [abstract]
19. Melichar B, Tabernero J, Casado E, Bridgewater J, Hamm J, Sklenar I, Holland J, Cheung W, Zaknoen S, Johri A (2005) Phase I dose optimization trial of patupilone in previously treated patients (pts) with advanced colon cancer (ACC). J Clin Oncol 23:292s
20. Naritomi Y, Terashita S, Kimura S, Suzuki A, Kagayama A, Sugiyama Y (2001) Prediction of human hepatic clearance from in vivo animal experiments and in vitro metabolic studies with liver microsomes from animals and humans. Drug Metab Dispos 29:1316–1324
21. O'Reilly T, McSheehy PMJ, Wenger F, Hattenberger M, Muller M, Vaxelaire J, Altmann KH, Wartmann M (2005) Patupilone (epothilone B, EPO906) inhibits growth and metastasis of experimental prostate tumors in vivo. Prostate 65:231–240
22. O'Reilly T, Wartmann M, Brueggen J, Allegrini PR, Floersheimer A, Maira M, McSheehy PMJ (2008) Pharmacokinetic profile of the microtubule stabilizer patupilone in tumor-bearing rodents and comparison of anti-cancer activity with other MTS in vitro and in vivo. Cancer Chemother Pharmacol 62:1045–1054
23. O'Reilly T, Wartmann M, Maira SM, Hattenberger M, Vaxelaire J, Muller M, Ferretti S, Buchdunger E, Altmann KH, McSheehy PMJ (2005) Patupilone (epothilone B, EPO906) and imatinib (STI571, Glivec) in combination display enhanced antitumour activity in vivo against experimental rat C6 glioma. Cancer Chemother Pharmacol 55:307–317
24. Obach RS (1999) Prediction of human clearance of twenty-nine drugs from hepatic microsomal intrinsic clearance data: an examination of in vitro half-life approach and nonspecific binding to microsomes. Drug Metabo Dispos 27:1350–1359
25. Ogiu N, Nakamura Y, Ijiri I, Hiraiwa K, Ogiu T (1997) A statistical analysis of the internal organ weights of normal Japanese people. Health Phys 72:368–383
26. Parrott N, Paquereau N, Coassolo P, Lave T (2005) An evaluation of the utility of physiologically based models of pharmacokinetics in early drug discovery. J Pharma Sci 94:2327–2343
27. Potchoiba MJ, West M, Nocerini MR (1998) Quantitative comparison of autoradioluminographic and radiometric tissue distribution studies using carbon-14 labeled xenobiotics. Drug Metab Dispos 26:272–277
28. Poulin P, Jones RD, Jones HM, Gibson CR, Rowland M, Chien JY, Ring BJ, Adkison KK, Ku MS, He H, Vuppugalla R, Marathe P, Fischer V, Dutta S, Sinha VK, Bjornsson T, Lave T, Yates JW (2011) PHRMA CPCDC initiative on predictive models of human pharmacokinetics, part 5: Prediction of plasma concentration-time profiles in human by using the physiologically-based

pharmacokinetic modeling approach. J Pharma Sci 100:4147–4157
29. Poulin P, Theil FP (2002) Prediction of pharmacokinetics prior to in vivo studies. 1. Mechanism-based prediction of volume of distribution. J Pharma Sci 91:129–156
30. Reese M, Sanchez-Pedregal VM, Kubicek K, Meiler J, Blommers MJJ, Griesinger C, Carlomagno T (2007) Structural basis of the activity of the microtubule-stabilizing agent epothilone A studied by NMR spectroscopy in solution. Angew Chem Int Ed Engl 46:1864–1868
31. Ring BJ, Chien JY, Adkison KK, Jones HM, Rowland M, Jones RD, Yates JW, Ku MS, Gibson CR, He H, Vuppugalla R, Marathe P, Fischer V, Dutta S, Sinha VK, Bjornsson T, Lave T, Poulin P (2011) PhRMA CPCDC initiative on predictive models of human pharmacokinetics, part 3: comparative assessment of prediction methods of human clearance. J Pharma Sci 94:1259–1276
32. Rodgers T, Leahy D, Rowland M (2005) Physiologically based pharmacokinetic modeling 1: predicting the tissue distribution of moderate-to-strong bases. J Pharma Sci 94:1259–1276
33. Rodgers T, Rowland M (2006) Physiologically based pharmacokinetic modelling 2: predicting the tissue distribution of acids, very weak bases, neutrals and zwitterions. J Pharm Sci 95:1238–1257
34. Rowland M, Peck C, Tucker G (2011) Physiologically-based pharmacokinetics in drug development and regulatory science. Annu Rev Pharmacol Toxicol 51:45–73
35. Rubin EH, Rothermel J, Tesfaye F, Chen T, Hubert M, Ho YY, Hsu CH, Oza AM (2005) Phase I dose-finding study of weekly single-agent patupilone in patients with advanced solid tumors. J Clin Oncol 23:9120–9129
36. Tanabe KM, Millward M, Allen JD (2005) Interactions of patupilone (Epothilone B) with multidrug transporter proteins. Proc Amer Assoc Cancer Res 46 [Abstract] 3430 AACR meeting
37. Ten Bokkel Huinink WW, Sufliarsky J, Smit WM, Spanik S, Wagnerova M, Hirte HW, Kaye S, Johri AR, Oza AM (2009) Safety and efficacy of patupilone in patients with advanced ovarian, primary fallopian, or primary peritoneal cancer: a phase I, open-label, dose-escalation study. J Clin Oncol 27:3097–3103
38. Tsimberidou AM, Lewis N, Reid T, Burris H, Urban P, Tan EY, Anand S, Uehara C, Kurzrock R (2011) Pharmacokinetics and antitumor activity of patupilone combined with midazolam or omeprazole in patients with advanced cancer. Cancer Chemother Pharmacol 68:1507–1516
39. Zatloukal P, Mellemgaard A, Sanchez JM, Perry MC, Hamm JT, Van Meerbeeck J, Deleo JJ, Gao B, Johri AR, Felip E (2008) Activity of patupilone in advanced or metastatic non-small cell lung cancer (Nsclc): a phase II study. J Clin Oncol. 2007 ASCO annual meeting proceedings part I, vol 25, no 18S (June 20 Supplement), 18058 [abstract]